KeAi
CHINESE ROOTS
GLOBAL IMPACT

Available online at www.sciencedirect.com

ScienceDirect

Advances in Climate Change Research 11 (2020) 349–359

www.keaipublishing.com/en/journals/accr/

Future changes of cluster high temperature events over China from RegCM4 ensemble under RCP4.5 scenario

ZHOU Bo-Tao[a,*], CHENG Yang[a,b], HAN Zhen-Yu[c], XU Ying[c], WANG Xiao-Long[d]

[a] *Collaborative Innovation Center on Forecast and Evaluation of Meteorological Disasters/Key Laboratory of Meteorological Disaster, Ministry of Education/Joint International Research Laboratory of Climate and Environment Change, Nanjing University of Information Science and Technology, Nanjing, 210044, China*
[b] *School of Atmospheric Sciences, Chengdu University of Information Technology, Chengdu, 610225, China*
[c] *National Climate Center, China Meteorological Administration, Beijing, 100081, China*
[d] *Zhengzhou Meteorological Service, Zhengzhou, 450000, China*

Received 25 May 2020; revised 7 August 2020; accepted 20 November 2020
Available online 2 December 2020

Abstract

Using the daily maximum temperature of the RegCM4 dynamical downscaling from four global climate models under the historical and RCP4.5 simulations, this study firstly identified the cluster high temperature event (CHTE) occurring in China through a simplified objective method, and then projected its change during the 21st century in terms of the CHTE metrics including frequency, duration, extreme intensity, cumulative intensity, maximum influential area, average influential area, and comprehensive intensity. The ensemble projection indicates that all the CHTE metrics tend to increase toward the end of the 21st century on the national scale. Besides, the occurrence of CHTE shows a longer month span during the middle and the end of the 21st century (from April to October) compared to the present (from April to September), accompanied with the peaks of the frequency, duration, and cumulative intensity shifting from the present July ahead to June. Relative to 1986–2005, the projected slight, moderate, and extreme CHTEs increase by 55%, 50%, and 50% (58%, 43%, and 60%) during 2046–2065 (2080–2099), respectively; the projected severe CHTE increases by 11% during 2046–2065 while decreases by 11% during 2080–2099. Spatially, the CHTE frequency, duration, and cumulative intensity are projected to increase in a widespread region. The largest increase appears in southern China for the frequency and in Xinjiang and Southeast China for the duration and cumulative intensity. We further divided China into five sub-regions to examine the regional features of CHTE changes. It is found that in addition to the increase of CHTEs in each single sub-region, a pronounced enhancement is also projected for the occurrence of cross-regional CHTEs, particularly for that across more than two sub-regions.

Keywords: Cluster high temperature event; Regional climate model; Dynamical downscaling; Ensemble projection

1. Introduction

Change in climate extremes is an issue of particular interest and major concern for scientists, policymakers and the public, since climate extremes exert profound impacts on agriculture, water resource, ecosystem and sustainable development (IPCC, 2012). According to the Fifth Assessment Report (AR5) of the Intergovernmental Panel on Climate Change (IPCC, 2013), the warm extremes have increased since the last half of the 20th century at global scale. A further increase toward the end of the 21st century is projected under the reprehensive concentration pathways (RCPs). The observed and projected change in temperature extremes over China in the context of global warming has also been well documented and similar results to the global scale have been achieved (e.g., Zhou et al., 2014; Zhou et al., 2016; Wang et al., 2017b; Shi et al., 2018; Sui et al., 2018; Xu et al., 2018; Wang et al., 2019b; Xie et al., 2020).

* Corresponding author.
E-mail address: zhoubt@nuist.edu.cn (ZHOU B.-T.).
Peer review under responsibility of National Climate Center (China Meteorological Administration).

https://doi.org/10.1016/j.accre.2020.11.007

However, those studies mostly focused on the temperature extreme indices defined by the Expert Team on Climate Change Detection and Indices (ETCCDI) (Klein et al., 2009; Zhang et al., 2011; Sillmann et al., 2013). Little attention has been shown to the cluster high temperature events (CHTEs). In fact, the CHTE usually persists for a long time and occurs over a large extent (Yang et al., 2010, 2012; Shi et al., 2011; Ren et al., 2012; Kuang et al., 2014; Wang et al., 2018). It can lead to more seriously adverse impacts on human health, ecosystem, and socio-economy. For instance, a CHTE occurring in eastern China in the summer time of 2018 lasted from July 9 to August 16. The area affected by the high temperature above 35 °C on July 20 reached 1607,000 km^2, involving 18 provinces (cities and districts) (Zhou et al., 2019). Thus, we are eager to know the secular change in CHTE under the background of global warming, which is of particular significance for adaptation. Kuang et al. (2014) indicated that the CHTE frequency, duration, and affected areas over China since 1961 has been the most pronounced after 2000, but it remains unknown how the CHTE will change in a warmer scenario.

On the other hand, the horizontal resolution of climate models exerts a certain effect on the projection of regional or local climate change (Gao et al., 2008; Lee et al., 2014; Jiang et al., 2016; Shi et al., 2017; Guo et al., 2018). Due to their coarse resolutions, global climate models (GCMs) may not capture some regional or local phenomena (Giorgi et al., 2009; Yao et al., 2017). To circumvent the limited resolution of GCMs, regional climate model (RCM) dynamical downscaling has been applied. RCMs with higher resolutions have been demonstrated to show a better description of climate statistics at regional or local scales (Gao et al., 2006; Kopparla et al., 2013; Yu et al., 2015; Gao and Giorgi, 2017). Keeping these in mind, we are motived to project the CHTE change in China using an ensemble of RCM (i.e., RegCM4) downscaling simulations under the RCP4.5 scenario.

2. Data and methods

The RegCM4 (Giorgi et al., 2012) downscaling simulations (CdR, EdR, HdR, MdR) for 1980–2100 are respectively driven by the four CMIP5 GCMs (CSIRO-Mk3.6.0, EC-EARTH, HadGEM2-ES, MPI-ESM-MR), in which 1980–2005 is for the historical simulation and 2006–2100 for the RCP4.5 simulation. The region for the downscaling covers the entire China and adjacent areas as recommended by the CORDEX-East Asia phase II (Giorgi et al., 2009). For the RegCM4, the horizontal resolution is set as 25 km and the vertical direction is divided into 18 layers with the top at 10 hPa. The selected parameterization schemes are the same as that introduced by Gao et al. (2016; 2018) and Han et al. (2017). The four CMIP5 GCMs used to drive RegCM4 are selected due to their high resolutions to match the 25 km grid spacing RCM and data availability (Han et al., 2017; Zhou et al., 2018). 1986–2005 is taken as the reference period for projection; 2046–2065 and 2080–2099 stand for the middle and the end of the 21st century, respectively. The arithmetic average of the four RegCM4 downscaling simulations is regarded as the ensemble mean (MME).

The daily maximum temperature (T_{max}) from the RegCM4 dynamic downscaling is used for the identification of CHTE. Following Kuang et al. (2014), the CHTE is identified by a simplified objective method. This objective method can measure the CHTE characteristics in terms of influential area, temporal continuity, and spatial cluster. The steps for the CHTE identification are as follows: i) detect the daily T_{max} in each grid. If the daily T_{max} is greater than 35 °C, it is regarded as extreme high temperature; ii) determine the maximum distance between adjacent lattice points (D_c) in the same event and the minimum number of lattice points (Q_c) in the event; iii) estimate the threshold of overlapping lattice points (H_c), and then compare the event on the given day with that on the previous day (named 'original event'). If the number of overlapping lattice points is more than H_c, the event on the given day is incorporated into the original event and the original event continues. If the number of overlapping lattice points is less than H_c, the event on the given day is regarded as a new event.

Cheng et al. (2020) determined the three parameters for the RegCM4 grid data via a total of 11 groups of tests. According to their study, the H_c, D_c, and Q_c are respectively set as 1, 40 km and 100 in this study. If an event with the daily T_{max} greater than 35 °C occurs over no less than 100 adjacent lattice points and persists no less than 5 d, and there is an overlapping in affected area by the extreme high temperature between the day before and the day after the given day, this event is identified as one CHTE.

Following Cheng et al. (2020), several metrics are also employed to quantatively measure the CHTE characteristics: the frequency (F) depicts the number of CHTEs; the duration (D) indicates the total number of days for a CHTE; the extreme intensity (I_e) and the cumulative intensity (I_c) represent the maximum of T_{max} among all lattice points and the sum of anomalies in T_{max} exceeding 35 °C at each lattice point during one CHTE process, respectively; the maximum influential area (A_M) and the average influential area (A_S) describe the maximum and mean area affected by one CHTE, respectively. The comprehensive intensity index (Z) is defined as

$$Z = 0.22 \times D' + 0.21 \times I_e' + 0.18 \times I_c' + 0.2 \times A_M' + 0.19 \times A_S' \quad (1)$$

where ' indicates the standardized value. The weight coefficient for each single index in the comprehensive intensity index is calculated as follows: Firstly, each single index are standardized and ranked in an ascending order. Then, the values of each single index at the 10th percentile interval are picked out and marked as $X_{i|j}$ ($i = 1 \ldots 5, j = 1 \ldots 10$) where i indicates the single index and j indicates the percentile. Following, the proportion of the 90th and 100th percentile

values (P_i) to the total percentile values is calculated in terms of the formula:

$$P_i = \frac{X_{i|j=9} + X_{i|j=10}}{\sum_{j=1}^{10} X_{i|j}} \quad (2)$$

and the weight coefficient (J_i) is finally obtained by

$$J_i = \frac{P_i}{\sum_{i=1}^{5} P_i} \quad (3)$$

According to Ren et al. (2012), the CHTE can be classified into four intensity levels based on the percentile thresholds: 10% (extreme), 20% (severe), 40% (moderate), and 30% (slight). These thresholds correspond to the range of Z index for the reference period: extreme CHTE ($Z \geq 0.88$), severe CHTE ($0.23 \leq Z < 0.88$), moderate CHTE ($-0.43 \leq Z < 0.23$), and slight CHTE ($Z < -0.43$), respectively.

We focus on the RegCM4 projected CHTE changes since Cheng et al. (2020) has validated good performance of the RegCM4 downscalings in simulating CHTEs in China. According to the regional distribution of CHTE under the current climatology, we divide China into five sub-regions (Fig. 1), Southeast China (SE), Southwest China (SW), North and Northeast China (NNE), western Northwest China (NWW), and eastern Northwest China (NWE). Southern China (SCN) indicates the region across SE and SW; eastern China (ECN) indicates the region across SE and NNE; northern China (NCN) indicates the region across NNE and NWE; western China (WCN) indicates the region across NWW and NWE; MCN refers to that the region covers no less than three sub-regions. All CHTEs can be classified into ten groups: five groups occurring only in one single sub-region, four groups occurring across two sub-regions, and one group occurring across more than two sub-regions.

3. Results

3.1. Temporal changes

Figure 2 shows the temporal evolution of the seven CHTE metrics averaged in China under the RCP4.5 scenario. A general increasing trend in the metrics is clearly observed for both the ensemble and individual projections. Except a flat change in the CHTE frequency after the middle of the 21st century (Fig. 2a), all the other indices are projected by the MME to increase persistently toward the end of the 21st century. Relative to the reference period (1986–2015), the MME projected percentage increases in F, D, I_e, I_c, A_M, and A_S are 44%, 33%, 1.2%, 170%, 59%, 38% for the middle of the 21st century (2046–2065), and 39%, 44%, 1.7%, 300%, 80%, and 55% for the end of the 21st century (2080–2099), respectively (also see the upper corner of Fig. 3).

The constitution of each CHTE metric at different scales to the total events over China is illustrated in Fig. 3. The result

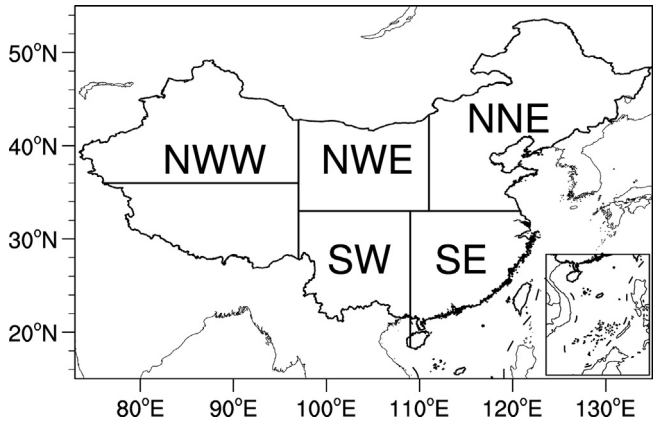

Fig. 1. Domains used, Southeast China (SE), Southwest China (SW), North and Northeast China (NNE), eastern Northwest China (NWE), and western Northwest China (NWW).

shows that the distribution pattern of the MME projected proportion under the RCP4.5 for each index is generally similar to that for the reference period. Salient changes at different scales between the future and the present are also noted. Compared with the reference period, the proportion of the CHTE duration longer than 21 d would increase during the middle and the end of the 21st century, with the largest increase of 5% in 2046–2065 and 7% in 2080–2099 for that exceeding 33 d. In contrast, the proportion of the CHTE duration less than 21 d is projected to decrease (Fig. 3a). The projected ratio of the CHTE with the I_e above 45 °C (below 40 °C) tends to increase (decrease) by 9% (6%) in 2046–2065 and further to 13% (8%) in 2080–2099 (Fig. 3b). For the CHTE with the I_c higher (lower) than 3×10^4 °C, an increase (a decrease) in its ratio is anticipated (Fig. 3c). For the CHTE with $A_M > 2.3 \times 10^6$ km^2, the ratio is projected to increase by 7% and 10% while a decrease of 10% and 12% is expected for that with $5 \times 10^5 < A_M \leq 8 \times 10^5$ km^2 by the middle and the end of the 21st century, respectively (Fig. 3d). The proportion of the CHET with $A_S > 7 \times 10^5$ km^2 is projected to increase, and the largest decrease is applicable for that with $1 \times 10^5 < A_S \leq 2 \times 10^5$ km^2 (Fig. 3e). In general, the proportion of the CHET falling into 'large value range' is expected to increase substantially, while that falling into 'small value range' is inclined to decrease.

We further examined the MME projected monthly changes of the CHTE indices during the middle and the end of the 21st century. As shown in Fig. 4a, due to the climate warming, the occurrence of CHTE tends to extend from September at the present to October in the middle and end of the 21st century, indicating a longer time span. Moreover, the proportion in April and September is anticipated to largely enhance with respect to the reference period. The CHTE duration is projected to prolong in the months from May to October, with the maximum increase of 6 d in June for 2046–2065 and further to 9 d for 2080–2099 as compared to 1986–2005 (Fig. 4b). The most significant change in I_c also appears in June, showing a three-fold increase by the middle of the 21st century and

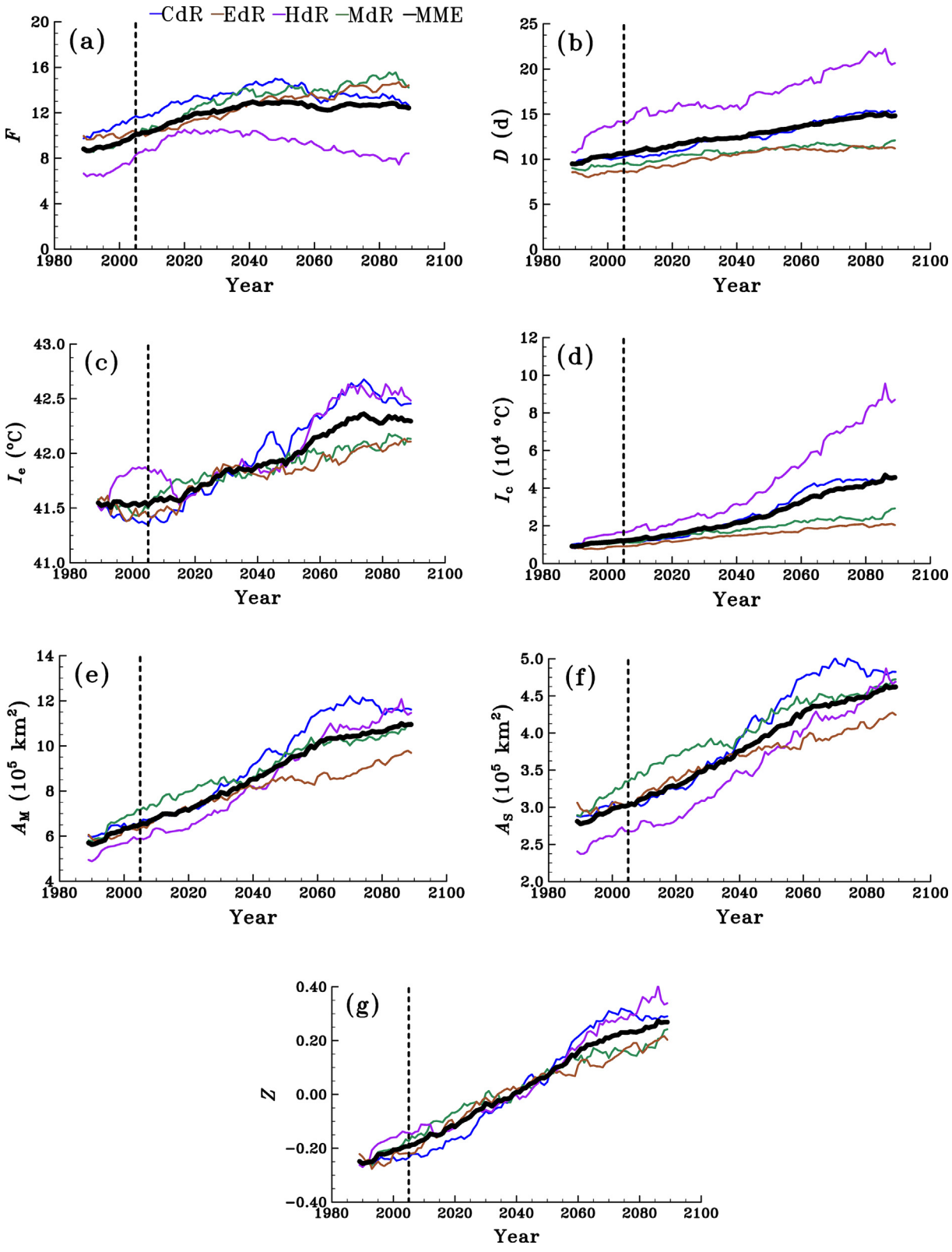

Fig. 2. Temporal evolution of (a) frequency (F), (b) duration (D), (c) extreme intensity (I_e), (d) cumulative intensity (A_M), (e) maximum influential area (A_S), (f) average influential area, and (g) comprehensive intensity (Z) of the CHTE over China (Time series is smoothed with a 20-year running mean filter). CdR, EdR, HdR, and MdR indicate the downscaling simulations driven by CSIRO-Mk3.6.0, EC-EARTH, HadGEM2-ES, MPI-ESM-MR, respectively, and MME indicates the ensemble mean of the four downscaling simulations.

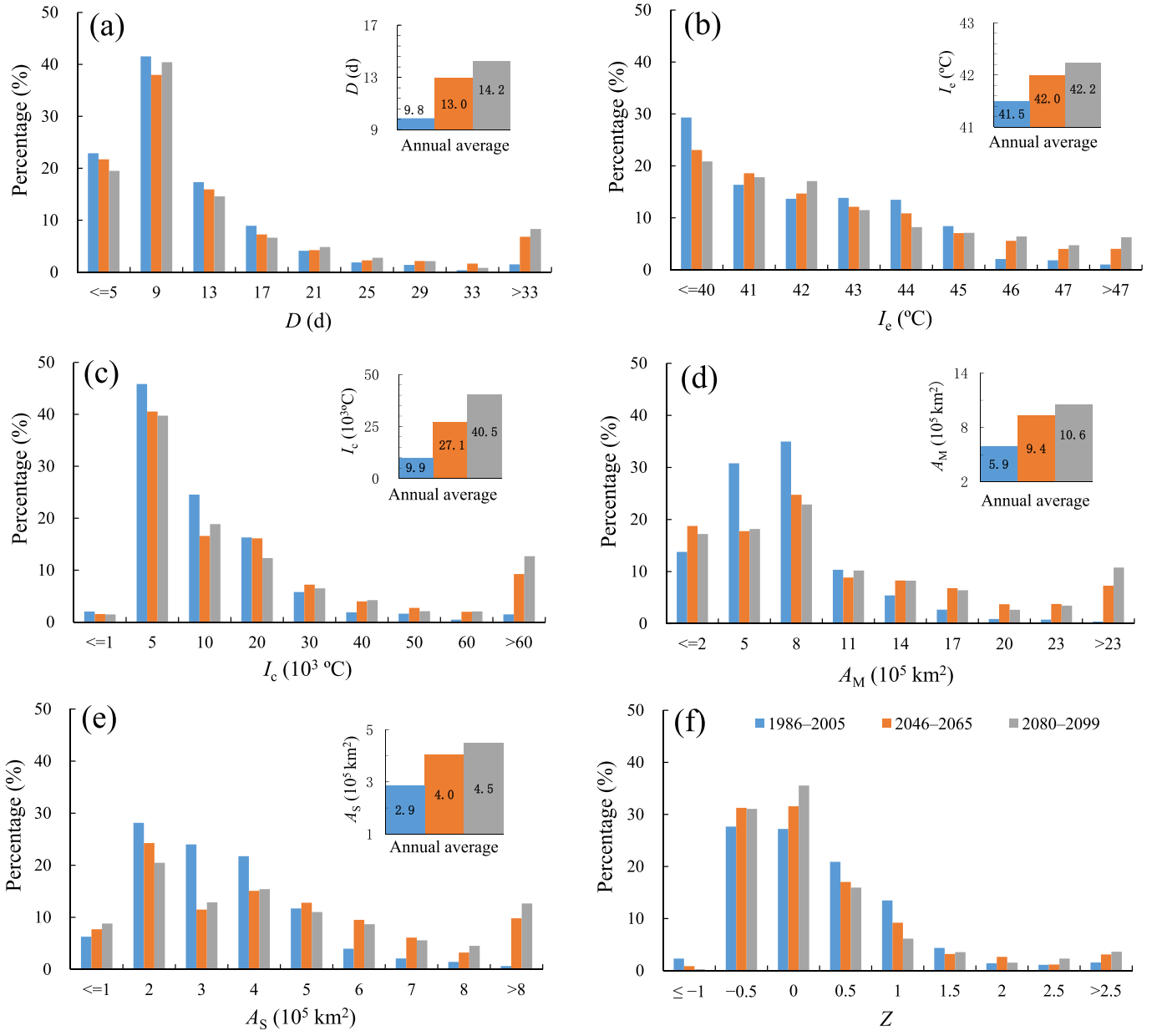

Fig. 3. MME simulated distribution of the percentage (%) of (a) duration, (b) extreme intensity, (c) cumulative intensity, (d) maximum influential area, (e) average influential area, and (f) comprehensive intensity of CHTEs at different scales to the total events over China. Annual average values of each CHTE metrics are shown in the upper-right corner of the panels (a–e).

a six-fold increase by the end of the 21st century (Fig. 4d). The A_M (Fig. 4e) and A_S (Fig. 4f) in June are projected to increase by 96% and 61% (1.4 times and 93%) over the course of 2046–2065 (2080–2099), respectively. In contrast, little change is projected for the I_e (Fig. 4c).

Figure 5 exhibits the MME projected changes of the frequencies of the four categories of CHTE and the ratio of each category to the total events. The projection indicates an increase in the slight, moderate, and extreme CHTEs during the middle and the end of the 21st century. Relative to the reference period, their respective frequencies are projected to increase by 55%, 50% and 50% during 2046–2065. The corresponding increases during 2080–2099 are 58%, 43% and 60%. The projected severe CHTE increases by 11% for 2046–2065 while decreases by 11% for 2080–2099. Because of different changes in the four categories of CHTEs, their ratios to the total events would change correspondingly. During the middle and the end of the 21st century, the proportion of the slight and moderate CHTEs to the total events is projected to increase.

3.2. Spatial patterns

Figure 6 displays the spatial distribution of the MME projected anomalies in the CHTE frequency, duration and cumulative intensity by the middle and end of the 21st century relative to the reference period. A widespread increase can be

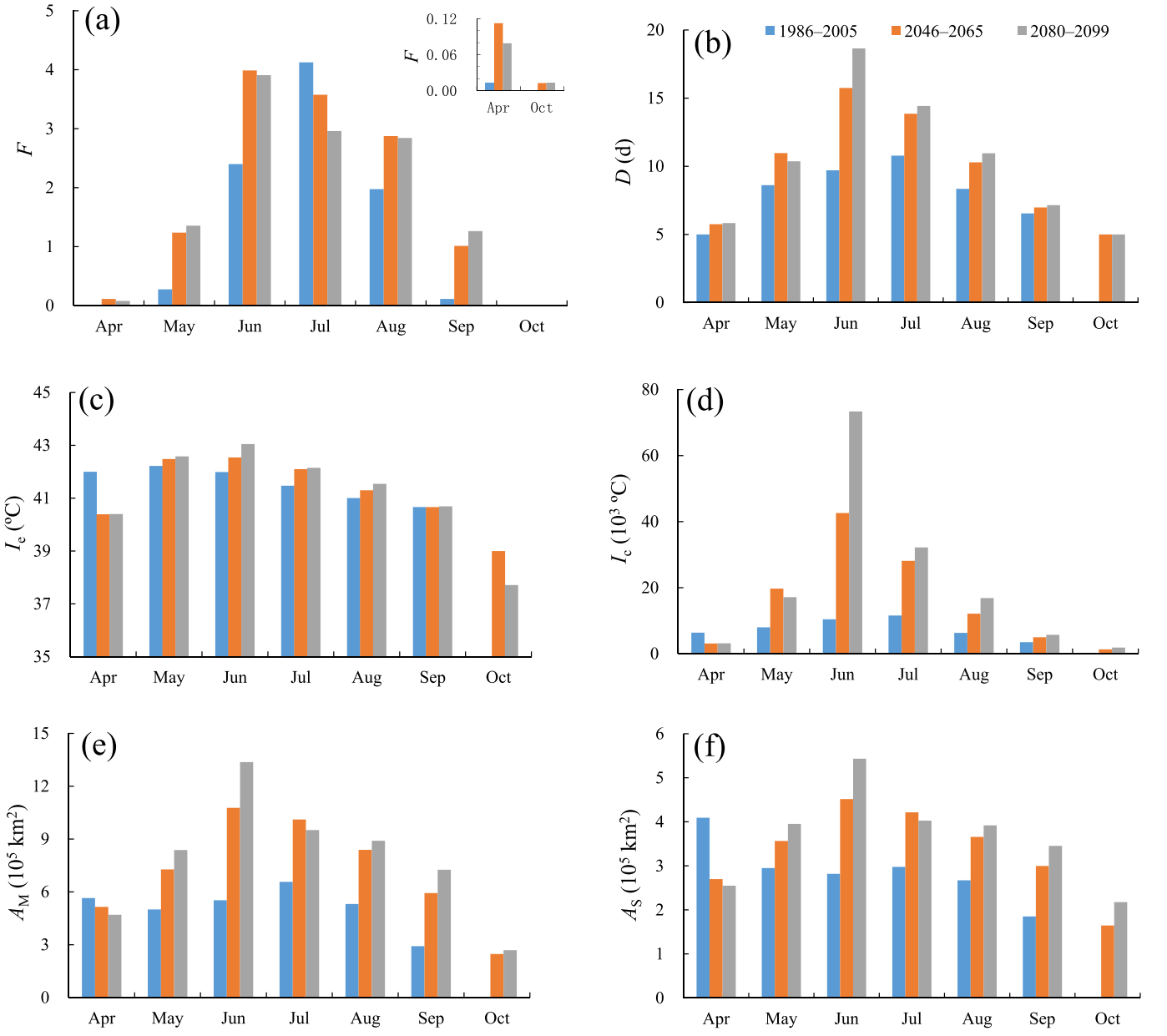

Fig. 4. MME simulated distribution of monthly (a) frequency, (b) duration, (c) extreme intensity, (d) cumulative intensity, (e) maximum influential area, and (f) average influential area of the CHTE over China. Given the small values, the CHTE frequencies in April and October are shown in the upper-right corner of the panel (a).

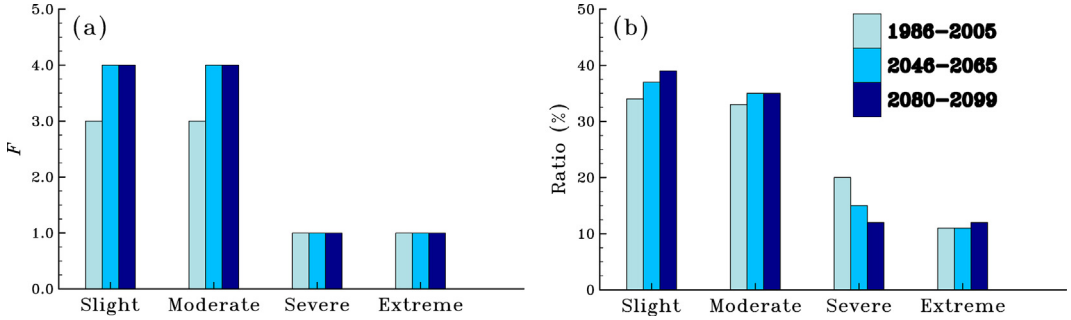

Fig. 5. MME simulated (a) annual mean frequencies of four CHTE categories and (b) ratio (%) of the four CHTEs to the total events over China.

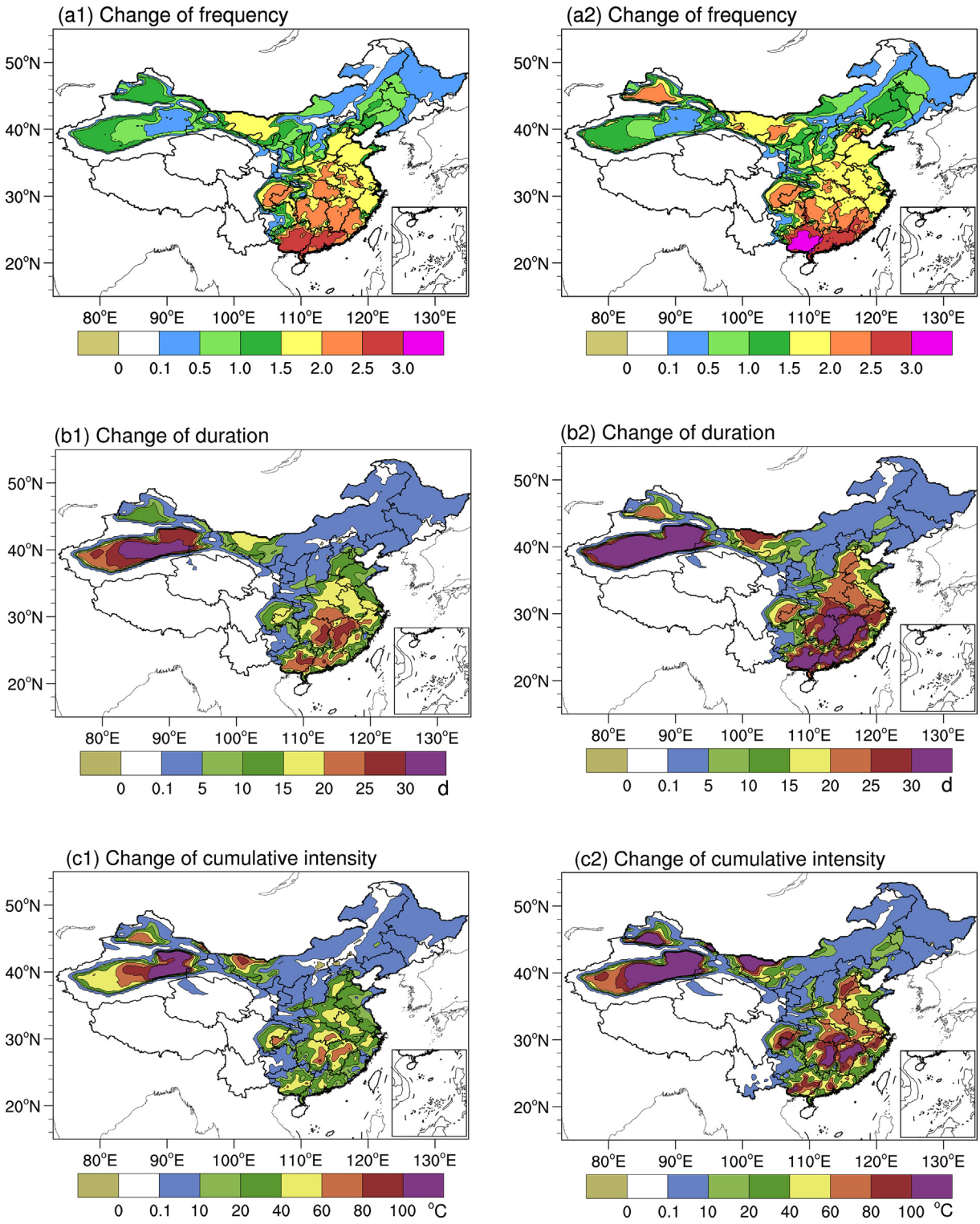

Fig. 6. MME projected changes (relative to 1986−2005) of annual mean (a1, a2) frequency, (b1, b2) duration, and (c1, c2) cumulative intensity of the CHTE during the middle (2046−2065) and the end (2080−2099) of the 21st century.

clearly found. The largest increase in the CHTE frequency occurs in parts of SCN, with the increasing magnitude being 2−3 times by the middle of the 21st century (Fig. 6a1) and 2.5−4 times by the end of the 21st century (Fig. 6a2). The greatest change in the CHTE duration, exceeding 30 d during the middle of the 21st century, occurs in southern Xinjiang located in NWW, followed by SE (20−25 d) (Fig. 6b1). The increase in these regions is further enhanced toward the end of

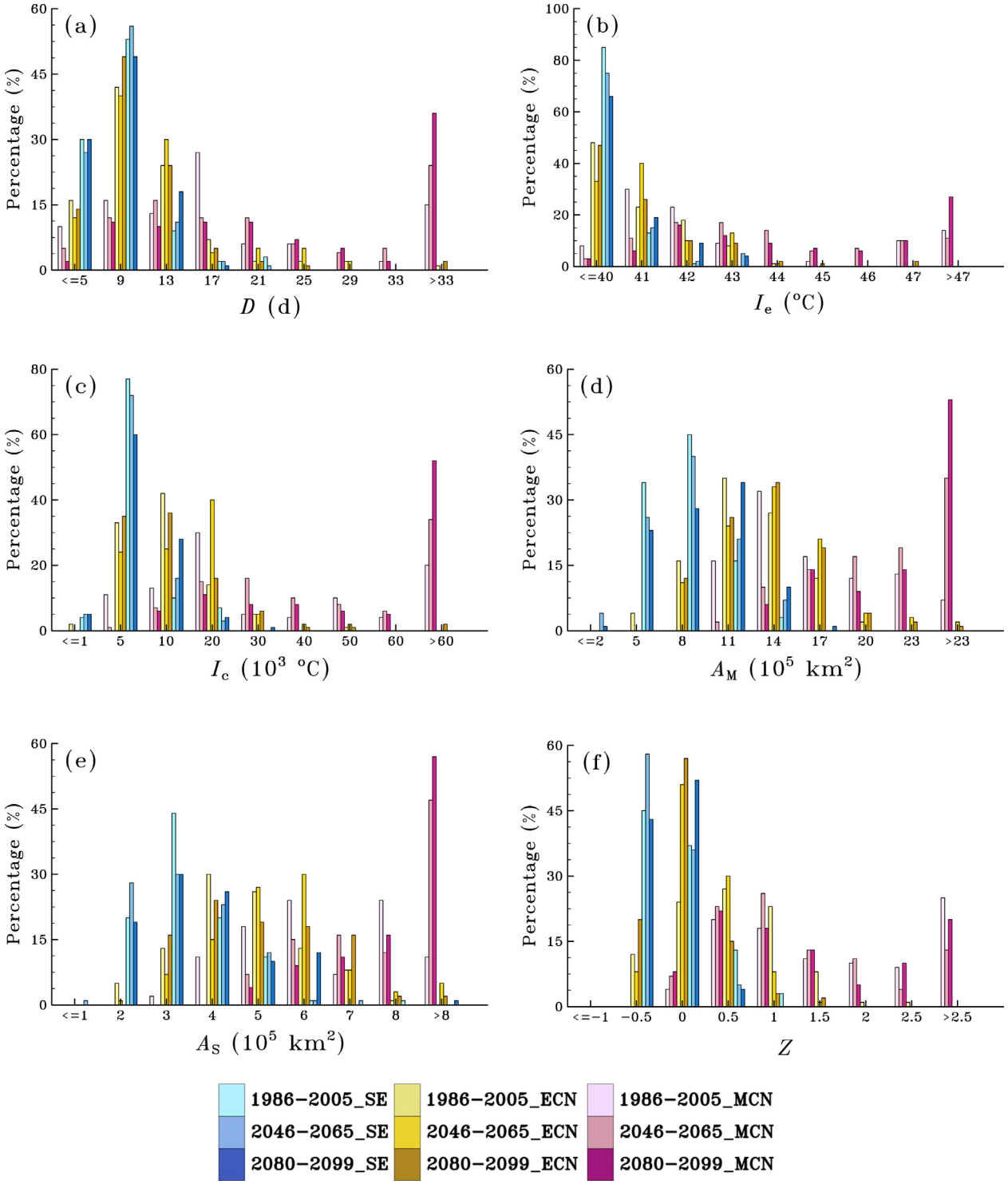

Fig. 7. MME simulated distribution of the percentage (%) of (a) duration, (b) extreme intensity, (c) cumulative intensity, (d) maximum influential area, (e) average influential area, and (f) comprehensive intensity of CHTEs at different scales to the total events over Southeast China (SE), eastern China (ECN), and the region covering no less than three sub-regions (MCN).

Table 1
MME simulated average frequency of CHTEs over different groups of sub-regions.

	Region	1986–2005	2046–2065	2080–2099
CHTEs only covering one single sub-region	SE	0.9	1.1	1.0
	SW	0.2	0.5	0.4
	NNE	0.3	0.5	0.5
	NWE	0.8	1.0	0.8
	NWW	4.7	4.8	4.8
CHTEs covering two sub-regions	SCN	0.2	0.5	0.7
	ECN	1.2	1.1	0.9
	NCN	0.1	0.1	0.2
	WCN	0.1	0.6	0.6
CHTE covering no less than three sub-regions	MCN	0.4	2.5	2.6
Total		8.9	12.8	12.4

Table 2
MME simulated mean value for each CHTE metrics over Southeast China (SE), eastern China (ECN), and the region covering no less than three sub-regions (MCN).

Index	SE			ECN			MCN		
	1986–2005	2046–2065	2080–2099	1986–2005	2046–2065	2080–2099	1986–2005	2046–2065	2080–2099
F	0.9	1.1	1.0	1.2	1.1	0.9	0.4	2.5	2.6
D (d)	7.3	7.4	7.2	10.3	10.5	10.5	18.8	25.9	35.5
I_e (°C)	39.1	39.3	39.6	40.0	40.5	40.4	42.6	43.6	44.5
I_c (10^4 °C)	0.4	0.4	0.5	0.9	1.2	1.5	4.4	8.8	16.7
A_M (10^5 km^2)	6.2	6.5	7.5	10.3	12.8	12.0	16.4	23.6	28.7
A_S (10^5 km^2)	2.8	2.8	3.3	4.1	5.0	4.6	6.1	8.5	10.4

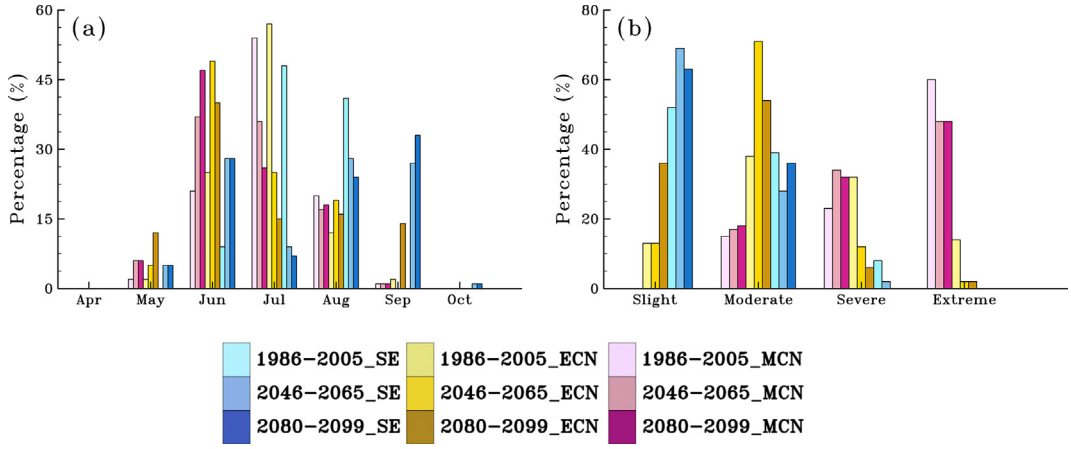

Fig. 8. MME simulated distribution of the percentage (%) of (a) monthly frequency and (b) the four CHTE categories to the total events over Southeast China (SE), eastern China (ECN), and the region covering no less than three sub-regions (MCN).

the 21st century (Fig. 6b2). The most significant change in the CHTE cumulative intensity appears in parts of Xinjiang and SE (Fig. 6c1 and Fig. 6c2).

The MME projected regional change of the frequencies for ten groups of CHTEs is summarized in Table 1. A general increase in the frequency is projected for all the CHTEs occurring only in a single sub-region. However, their ratio to the total frequency is projected to decrease in NWW, NWE, and SE during the middle and end of the 21st century. This may be due to the increase in the CHTEs across sub-regions. For example, the projected increase of the frequency is greater in WCN and SCN, particularly in MCN where the CHTE frequency is projected to occur from once every two or three years at the present to the two or three times per year by the end of the 21st century. Its proportion to the total frequency is enhanced from 4% of the reference period to 19% during 2046–2065 and further to 21% during 2080–2099.

Considering the CHTE distribution in different sub-regions as well as the regional population density and economic development, we performed further analysis on the characteristics of CHTE in SE, ECN, and MCN (Fig. 7). Generally, the CHTE indices are mainly distributed in the ‘small value range’ for SE (one single sub-region), in the ‘small and median value range’ for ECN (across two sub-regions), and in the

'large value range' for MCN (across more than two sub-regions).

Table 2 quantifies the changes of the CHTE indices in SE, ECN, and MCN. Relative to the reference period, in MCN, the projected D increases by 7 d during 2046–2065 and by 17 d during 2080–2099; the I_e increase by 1 °C and 1.9 °C and the I_c shows one-fold increase and 2.8-fold increase over the course of 2046–2065 and 2080–2099, respectively; the A_M (A_S) extends by 44% (39%) during 2046–2065 and further to 75% (70%) during 2080–2099. The CHTE in ECN displays an increase in I_c, A_M and A_S by 33%, 24%, 17% during 2046–2065 and 67%, 22%, and 12% during 2080–2099, respectively, while the projected changes in D and I_e are less than 2%. Little changes are projected for CHTE indices in SE except that the A_M (A_S) increases by 21% (18%) at the end of the 21st century.

Figure 8a shows the distribution of the percentage of monthly CHTEs to the total events in SE, ECN, and MCN. It can be noted that the highest frequency of CHTE in MCN and ECN tends to shift from the present July to June toward the end of the 21st century. Large increase of the CHTE frequency in SE is projected to mainly occur in June and September. Moreover, the CHTEs in MCN are basically severe and extreme events; the CHTE in ECN are usually moderate events; and the CHTE in SE are mostly slight and moderate events (Fig. 8b).

4. Conclusions and discussion

Based on a set of RegCM4 dynamical downscalings that were driven from four GCMs under the historical and RCP4.5 simulations, we identified the CHTEs in China by a simplified objective method. The main findings are summarized below:

(1) The ensemble of the RegCM4 dynamic downscalings projects an increasing tendency toward the end of the 21st century in the frequency, duration, extreme intensity, cumulative intensity, maximum influential area, average influential area, and comprehensive intensity of the CHTE over China under the RCP4.5 scenario.

(2) Among the CHTEs, the constitution of the events with the properties such as $D > 21$ d, $I_e > 45$ °C, $I_c > 3 \times 10^4$ °C, $A_M > 2.3 \times 10^6$ km^2, and $A_S > 7 \times 10^5$ km^2 is projected to enhance, generally accompanied with larger enhancement by the end of the 21st century than by the middle of the 21st century. As for the comprehensive intensity, relative to 1986–2005, the frequencies of slight, moderate, and extreme CHTEs are expected to increase by 55%, 50%, and 50% during 2046–2065, and 58%, 43%, and 60% during 2080–2099, respectively, while the projected severe CHTE increases in the former period and decreases in the latter period.

(3) At the monthly scale, a longer time span is projected for the CHTE occurrence during the middle and end of the 21st century (April to October) with respect to the present (April to September). Meanwhile, the peaks of the frequency, duration, and cumulative intensity shift ahead to June during the middle and late 21st century from the present July.

(4) Spatially, a widespread increase in the CHTE frequency, duration, and cumulative intensity are projected, with the largest increase in southern China for the frequency and in Xinjiang and Southeast China for the duration and cumulative intensity. In addition, the cross-regional CHTEs are projected to increase remarkably.

It should be noted that this study aims at the projected changes in CHTEs over China. The physical causes for their changes are not addressed. Given that our results reflect a possible estimate of CHTE changes as a response to future warming, the warming scenario is of course a main driver for its change. However, the detailed physical mechanisms responsible for different behaviors of CHTE metrics in different regions are rather complicated, since the occurrence of extreme high temperature is also influenced by the internal variability of climate system, such as atmospheric high-pressure system, land process, and sea surface temperature (e.g., Luo and Lau, 2017; Wang et al., 2017a; Chen and Zhou, 2018; Chen et al., 2019). Thus, this issue deserves further in-depth investigation in the future to get a full picture for the understanding of the CHTE change. In addition, the CHTE is identified based on the daily maximum temperature. Nevertheless, what human feel is the wet-bulb temperature, which also considers moisture. Combining daily temperature and humidity, Wang et al. (2019a) made a detailed analysis on the extreme wet-bulb temperature events in China and highlighted the important role of moisture in the extreme wet-bulb temperature events. Overall, moisture contributes more than temperature to extreme wet-bulb temperature events especially in North and Northwest China, and the temperature-dominated extreme wet-bulb temperature events tend to last longer than the moisture-dominated extremes. Given the significant role of moisture in extreme wet-bulb temperature events, the cluster of the compound events with the concurrence of temperature and moisture is also an interesting topic.

Considering the feature of CHTEs with a widespread spatial extent and a long persistence, the projected increase of CHTEs in a warmer scenario would impose more serious risks on human health and socio-economy than the non-cluster extreme temperature events. For example, as the increase of CHTEs, the cooling demand for habitant comfortability is expected to largely increase, which would load heavy burden on the electricity power sector and also increase energy consumption. The challenge associated with the change in CHTE raises the necessity and urgency for actions to develop adaptation and mitigation measurements.

Declaration of competing interest

The authors declare that they have no conflict of interest.

Acknowledgments

This research was jointly supported by the National Key Research and Development Program of China (2018YFA0606301) and the National Natural Science Foundation of China (41991285 and 42025502).

References

Chen, R., Wen, Z., Lu, R., et al., 2019. Causes of the extreme hot midsummer in central and South China during 2017: role of the western tropical Pacific warming. Adv. Atmos. Sci. 36 (5), 465−478.

Chen, X., Zhou, T., 2018. Relative contributions of external SST forcing and internal atmospheric variability to July−August heat waves over the Yangtze River valley. Clim. Dynam. 51, 4403−4419.

Cheng, Y., Zhou, B., Han, Z., et al., 2020. Evaluation of multi-RegCM4 dynamical downscaling simulations on cluster high temperature events in China. Clim. Change Res. https://doi.org/10.12006/j.issn.1673-1719.2019.226 (in Chinese).

Gao, X., Giorgi, F., 2017. Use of the RegCM system over East Asia: review and perspectives. Engineering 3 (5), 766−772.

Gao, X., Shi, Y., Giorgi, F., 2016. Comparison of convective parameterizations in RegCM4 experiments over China with CLM as the land surface model. Atmos. Oceanogr. Sci. Libr. 9, 246−254.

Gao, X., Xu, Y., Zhao, Z., et al., 2006. On the role of resolution and topography in the simulation of East Asia precipitation. Theor. Appl. Climatol. 86, 173−185.

Gao, X., Shi, Y., Song, R., et al., 2008. Reduction of future monsoon precipitation over China: comparison between a high resolution RCM simulation and the driving GCM. Meteorol. Atmos. Phys. 100, 73−86.

Gao, X., Wu, J., Shi, Y., et al., 2018. Future changes in thermal comfort conditions over China based on multi-RegCM4 simulations. Atmos. Oceanogr. Sci. Libr. 11 (4), 291−299.

Giorgi, F., Jones, C., Asrar, G., 2009. Addressing climate information needs at the regional level: the CORDEX framework. World Meteorol. Organ. Bull. 58, 175−183.

Giorgi, F., Coppola, E., Solmon, F., et al., 2012. RegCM4: model description and preliminary tests over multiple CORDEX domains. Clim. Res. 52, 7−29.

Guo, J., Huang, G., Wang, X., et al., 2018. Dynamically-downscaled projections of changes in temperature extremes over China. Clim. Dynam. 50, 1045−1066.

Han, Z., Zhou, B., Xu, Y., et al., 2017. Projected changes in haze pollution potential in China: an ensemble of regional climate model simulations. Atmos. Chem. Phys. 17, 10109−10123.

IPCC, 2012. Managing the Risks of Extreme Events and Disasters to Advance Climate Change Adaptation. Cambridge University Press, Cambridge and New York.

IPCC, 2013. Climate Change 2013: the Physical Science Basis. Contribution of Working Group I to the Fifth Assessment Report of the Intergovernmental Panel on Climate Change. Cambridge University Press, Cambridge and New York.

Jiang, D., Tian, Z., Lang, X., 2016. Reliability of climate models for China through the IPCC third to fifth assessment reports. Int. J. Climatol. 36, 1114−1133.

Klein Tank, A.M.G., Zwiers, F.W., Zhang, X., 2009. Guidelines on analysis of extremes in a changing climate in support of informed decisions for adaptation. Climate Data and Monitoring, WCDMP No.72. World Meteorological Organization, Geneva.

Kuang, X., Wang, Z., Zhang, Y., et al., 2014. Identification and statistical characteristics of the cluster high temperature events during last fifty years. Chin. J. Geophys. 57 (6), 1782−1791 (Chinese).

Kopparla, P., Fischer, E.M., Hannay, C., et al., 2013. Improved simulation of extreme precipitation in a high-resolution atmosphere model. Geophys. Res. Lett. 40, 5803−5808.

Lee, J.W., Hong, S.Y., Chang, E.C., et al., 2014. Assessment of future climate change over East Asia due to the RCP scenarios downscaled by GRIMs-RMP. Clim. Dynam. 42, 733−747.

Luo, M., Lau, N.C., 2017. Heat waves in southern China: synoptic behavior, long-term change, and urbanization effects. J. Clim. 30, 703−720.

Ren, F., Cui, D., Gong, Z., et al., 2012. An objective identification technique for regional extreme events. J. Clim. 25, 7015−7027.

Shi, C., Jiang, Z., Chen, W., et al., 2018. Changes in temperature extremes over China under 1.5°C and 2°C global warming targets. Adv. Clim. Change Res. 9, 120−129.

Shi, X., Lu, C., Xu, X., 2011. Variability and trends of high temperature, high humidity, and sultry weather in the warm season in China during the period 1961-2004. J. Appl. Meteor. Climatol. 50 (1), 127−143.

Shi, Y., Wang, G., Gao, X., 2017. Role of resolution in regional climate change projections over China. Clim. Dynam. 51, 2375−2396.

Sillmann, J., Kharin, V.V., Zhang, X., et al., 2013. Climate extremes indices in the CMIP5 multimodel ensemble: part I. model evaluation in the present climate. J. Geophys. Res. 118 (4), 1716−1733.

Sui, Y., Lang, X., Jiang, D., 2018. Projected signals in climate extremes over China associated with a 2°C global warming under two RCP scenarios. Int. J. Climatol. 38, e678−e697. https://doi.org/10.1002/joc.5399.

Wang, P., Tang, J., Sun, X., et al., 2017a. Heat waves in China: definitions, leading patterns, and connections to large-scale atmospheric circulation and SSTs. J. Geophys. Res. 122, 10679−10699.

Wang, P., Tang, J., Wang, S., et al., 2018. Regional heatwaves in China: a cluster analysis. Clim. Dynam. 50 (5), 1901−1917.

Wang, P., Leung, L.R., Lu, J., et al., 2019a. Extreme wet-bulb temperatures in China: the significant role of moisture. J. Geophys. Res. 124, 11944−11960.

Wang, X., Jiang, D., Lang, X., 2019b. Extreme temperature and precipitation changes associated with four degree of global warming above pre-industrial levels. Int. J. Climatol. 39, 1822−1838.

Wang, Y., Zhou, B., Qin, D., et al., 2017b. Changes in mean and extreme temperature and precipitation over the arid region of northwestern China: observation and projection. Adv. Atmos. Sci. 34, 289−305.

Xie, W., Zhou, B., You, Q., et al., 2020. Observed changes in heat waves with different severities in China during 1961–2015. Theor. Appl. Climatol. 141, 1529−1540.

Xu, Y., Gao, X., Giorgi, F., et al., 2018. Projected changes in temperature and precipitation extremes over China as measured by 50-year return values and periods based on CMIP5 ensemble. Adv. Atmos. Sci. 35, 376−388.

Yang, P., Hou, W., Feng, G., 2010. A study of the characteristics of the cluster extreme events in China. Clim. Environ. Res. 15 (4), 365−370 (Chinese).

Yang, P., Hou, W., Feng, G., 2012. The characteristics of clusters of weather and extreme climate events in China during the past 50 years. Chin. Phys. B 1, 553−561.

Yao, J., Zhou, T., Guo, Z., et al., 2017. Improved performance of high-resolution atmospheric models in simulating the East-Asian summer monsoon rainbelt. J. Clim. 30, 8825−8840.

Yu, E., Sun, J., Chen, H., et al., 2015. Evaluation of a high-resolution historical simulation over China: climatology and extremes. Clim. Dynam. 45, 2013−2031.

Zhang, X., Alexander, L., Hegerl, G.C., et al., 2011. Indices for monitoring changes in extremes based on daily temperature and precipitation data. Wiley Interdiscip. Rev. Climate Change 2, 851−870.

Zhou, B., Wen, H.Q., Xu, Y., et al., 2014. Projected changes in temperature and precipitation extremes in China by the CMIP5 multimodel ensembles. J. Clim. 27, 6591−6611.

Zhou, B., Xu, Y., Wu, J., et al., 2016. Changes in temperature and precipitation extreme indices over China: analysis of a high-resolution grid dataset. Int. J. Climatol. 36, 1051−1066.

Zhou, B., Wang, Z., Shi, Y., et al., 2018. Historical and future changes of snowfall events in China under a warming background. J. Clim. 31, 5873−5889.

Zhou, X., Zeng, H., Wang, Z., et al., 2019. Climatic characteristics and major meteorological events over China in 2018. Meteorol. Mon. 45 (4), 543−552 (Chinese).